SELECTION OF A PHOTOBLEACHING MODEL USING NONLINEAR REGRESSION ANALYSIS FOR APPLICATIONS IN QUANTITATIVE FLUORESCENCE MICROSCOPY IMAGING

J. Diaz-Zamboni*, V. H. Casco.

Laboratorio de Microscopia Aplicada a Estudios Moleculares y Celulares - Facultad de Ingeniería - Universidad Nacional de Entre Ríos - Oro Verde, Argentina

*Autor de correspondencia: Javier Eduardo Diaz-Zamboni, e-mail: javierdiaz@bioingenieria.edu.ar Tlf: 54 343 4975100 (interno 120), Fax: 54 343 4975100 (interno 105).

Recibido: Agosto 2012. Aprobado: Febrero 2013.
Publicado: Mayo 2013.

ABSTRACT
Fluorescence microscopy does constitute an essential tool in cellular and molecular biology research as well as in materials science. This technique permits to study both living cells dynamics in a noninvasive way or fixed cells, providing large amount of quantitative information. However, the technique is significantly affected by the photobleaching of fluorescent substances. This phenomenon is a photochemical transformation that occurs in different extent, in fluoresce molecules, and diminishing its ability to produce fluorescence, and thus reducing the signal to noise ratio in final images. In order to establish a model that allows explaining the phenomenon and providing information for the quantitative analysis of images, we analyzed four commonly models used in microscopy of exponential fluorescence decay. These were compared objectively using analysis of variance, being the function of four-parameter bi-exponential without constant term the model that best fit the data.

Keywords: Fluorescence microscopy, photobleaching, nonlinear regression, F-test.

SELECCIÓN DE UN MODELO DE FOTODECAIMIENTO UTILIZANDO ANÁLISIS DE REGRESIÓN NO LINEAL PARA APLICACIONES EN IMÁGENES DE MICROSCOPIA DE FLUORESCENCIA CUANTITATIVA

RESUMEN
La microscopía de fluorescencia es una herramienta fundamental en las investigaciones de biología molecular y celular así como también en ciencias de los materiales. Permite estudiar tanto la dinámica de células vivas de una manera prácticamente no invasiva, como las células fijadas. Sin embargo, la técnica se ve afectada por el fotodecaimiento de las sustancias fluorescentes. Este fenómeno consiste en una transformación fotoquímica que se produce en la moléculas que producen fluorescencia, disminuyendo su capacidad de producir fluorescencia y por lo tanto, reduciendo la relación señal ruido en la imágenes finales. Para establecer un modelo explicativo del fenómeno y proveer de información para el análisis cuantitativo de imágenes, se analizaron cuatro modelos de decaimiento exponencial de la fluorescencia comúnmente utilizados en microscopia. Estos se compararon de forma objetiva utilizando una prueba F sobre los residuos del ajuste de los modelos, obteniéndose que la función bi-exponencial de cuatro parámetros sin término constante resultó el modelo que mejor representa los datos.

Palabras claves: Microscopia de fluorescencia, fotodecaimiento, regresión no lineal, prueba F.

INTRODUCTION

Fluorescence microscopy is based on the fluorescence property of some substances to absorb photons of a specific wavelength and emitting to longer ones. The difference between these two wavelengths is called the

Stokes shift and is a particular property of fluorescence that makes it an extremely useful phenomenon [1, 2] since it does allow to optically separate the excitation from emission light. The substances that naturally produce fluorescence are called fluorophores, molecules generally composed of aromatic rings and in which, the outermost electrons determine their efficiency as a fluorescent compounds, and their wavelengths of absorption and emission. These substances are used in specific localization of cellular structures, which is achieved through various techniques such as biochemical, molecular, genetic and nano-technological. For example, it is possible to label almost any protein of a cell through an immune response, where the antigen is the protein to be targeted, and the antibody is the protein bearing the fluorophore. This technique is widely used and is known as immunofluorescence (IF). Another way to localize cell structures in a highly specific way is using fluorescent proteins such as Green Fluorescent Proteins (GFP) which can be inserted into gene constructs by genetic engineering that encode the target proteins, but these are neither structurally or functionally modified.

Although fluorescence microscopy permits to obtain very clear and highly-contrasted images, it is a microscopy mode that has degradation sources that normally are not present in other optical microscopies. This makes that the requirements for fluorescence measurement on images, through detected intensities, need an accurate instrument calibration, as well as precise control and reduced aberrations of the optical system. One of the more important image degradation sources in fluorescence microscopy is the photobleaching. This phenomenon consists in a fluorophore's photochemical transformation, which diminishes its ability to produce fluorescence, reducing the signal-noise ratio on the final images. This is a multifactorial process, among them we can mention the presence of oxygen into the sample, the intensity level of the incident radiation and the chemical composition of the environment in which the fluorophore is immersed [2, 4].

Therefore, fluorescence degradation level due to photobleaching is a key factor to take into account when quantitative fluorescence microscopy is required. It should also take into consideration in deconvolution process, because the vast majority of deconvolution algorithms are built from image formation models that only consider different noise models and background levels. In this case, photobleaching would be violating the linearity assumption of the model.

In this work we have applied a methodology to select from four photobleaching models used in fluorescence microscopy, the best describes the data. These models are represented by equations from (1) to (4).

$$i = \theta_1 e^{\theta_2 t} \quad (1)$$

The model given by equation (1) is the simplest form of photobleaching after linear regression, where θ_1 is proportional to the initial concentration of fluorophores, θ_2 is the decay-rate constant of the fluorescence and i is the intensity detected by the sensor.

$$i = \theta_1 e^{\theta_2 t} + \theta_3 \quad (2)$$

The model represented by equation (2) is similar to the that of equation (1), but it adds a parameter θ_3 that models the mean level of the background fluorescence [5, 6].

$$i = \theta_1 e^{\theta_2 t} + \theta_3 e^{\theta_4 t} \quad (3)$$

Equation (3) represents a model that considering two fluorophore populations with initial concentrations θ_1 and θ_3, and their decay-rate constants θ_2 and θ_4 [4].

$$i = \theta_1 e^{\theta_2 t} + \theta_3 e^{\theta_4 t} + \theta_5 \quad (4)$$

Finally, equation (4) is a model that adds to equation (3) the parameter θ_5, which represents the mean level of the background fluorescence.

Models described by equations (1) to (4) are nested. That is, simpler models are versions of the general models with at least a parameter equal to zero. Therefore, model

represented by equation (3) is nested in to the model of the equation (4), where the parameter θ_5=0. In the same way, models described by equations (2) and (1) are also nested in model of the equation (4) with θ_5=0 and, θ_4=0 and θ_3=0, respectively; and so on. This relationship between models will be very useful as we will show later.

We first define the general form of the mean function for the nonlinear regression:

$$E(I|T=t)=m(t,\theta) \quad (5)$$

where E is the expected-value operator, I is the set of all measurements i_j given the data predictors $\boldsymbol{t}_j$, with j=1...N, and being m the kernel mean function dependent of the unknown parameter vector $\boldsymbol{\theta}$.

As with linear models, we define the variance function which is given by:

$$Var(I|T=t_j)=\sigma^2/\omega_j \quad (6)$$

where ω_j are known positive weights and σ^2 is an unknown positive number. Equations (5) and (6) together with the assumption that observations are independent of each other define the nonlinear regression model [7, 8]. Taken this assumptions, we can use the least square technique to estimate the unknown parameters, minimizing over all permitted values of $\boldsymbol{\theta}$ the residual sum of squares function.

$$RSS(\theta)=\sum_{j=1}^{N}\omega_j\left(i_j-m(t_j,\theta)\right)^2 \quad (7)$$

By performing a comparison between linear and nonlinear regression, when minimizing *RSS* with respect to $\boldsymbol{\theta}$, the derivatives in linear regression is only data's dependent. In the nonlinear case, deriving *RSS* respect to $\boldsymbol{\theta}$, at least one of the derivatives is function of at least one parameter. In (multiple) linear regression an objective way to select one model, from a set, that represents the data, is by checking if an additional term append to the model will reduce significantly the residuals. This is an objective way to apply the principle of the Ockham's razor, where the purpose is to chose, from a set of models that equally describe the data, the simplest one. Then, as in multiple linear regressions, in nonlinear regression if the models are nested an F-test can be applied by building the following statistic:

$$F=\frac{\left(RSS_N(\theta_N)-RSS_G(\theta_G)\right)/(df_N-df_G)}{RSS_N/df_N} \quad (8)$$

where $\boldsymbol{\theta}_G$ is the vector of estimated parameters of a more general model, $\boldsymbol{\theta}_N$ is the vector of the estimated parameters of a simpler model which is nested in the general model. df_G and df_N are the degree of freedom of the general and nested model, respectively. Following, using the statistic given by equation (8), is possible to quantify the change in the sum of the square residuals of the models, using the p-value obtained from a F distribution with (df_N-df_G, df_N) degree of freedom [7, 9].

In our study, the kernel mean function *m,* (5), can be any of the equations from (1) to (4), and the unknown parameter vector $\boldsymbol{\theta}$ is formed by (θ_1, θ_2), (θ_1, θ_2, θ_3), (θ_1, θ_2, θ_3, θ_4) and (θ_1, θ_2, θ_3, θ_4, θ_5), respectively. The matrix of predictors $\boldsymbol{t}$ is formed by only one sample vector of exposition times to ultraviolet (UV) light; and each element t_j of $\boldsymbol{t}$ has a pair i_j which is the intensity imaged on a pixel.

In this manner, the set of time-sequential images captured is a sample of the fluorescence photobleaching of a portion of the an immuno-tagged specimen continuously exposed to UV-light.

MATERIALS AND METHODS

The specimen selected to this work was Rhinella arenarum tadpoles, which were obtained by in vitro fertilization. Adult males and females were kept in water at 20 °C for 24 hs, after which females were injected with 2500 IU of human chorionic gonadotropin (hCG) hormone (Endocorion, Elea, Buenos Aires). Twelve hours

later, eggs were harvested and fertilized with testis extracts as described by Rengel et al. [10].

Developmental stages were determined according to Gosner (1960) [11]. Stage 20 Rinhella arenarum tadpoles were fixed in Carnoy solution (ethanol:chloroform:acetic acid, 6:3:1), washed in PBS (Phosphate Buffered Saline), progressively dehydrated in ethanolic solutions of increasing concentrations (Cicarelli, Buenos Aires, Argentina) and xylol cleared (Cicarelli). Specimens were pre-included in xylol:paraffin 1:1, followed by six changes of paraffin (Cicarelli) and were finally included in pure paraffin. A Reichert Jung Hn 40 microtome was employed to obtain 5 μm-thick transversal sections from paraffin-embedded tissues, which were mounted on 1% gelatin-coated slides and dried at room temperature.

The monoclonal antibody 5D3 is a mouse IgG1 (chicken, frog) directed to the extracellular domain of the 120 kDa isoform of the cell-cell adhesion molecule E-cadherin (Transduction Laboratories, Lexington, Kentucky, USA). The antibody was used in a 1:50 dilution. For the detection of primary antibody binding, we used a secondary antibody (FITC-conjugated goat anti- mouse IgG; Sigma Chemical Company, St. Louis, USA) at a 1:64 dilution.

E-cadherin immunolocalization: sections were xylol-deparaffinated, hydrated in a descending-concentration alcohol series, methanol-treated with a 0,3 % solution of hydrogen peroxide to block endogenous peroxidase for 20 minutes at room temperature, washed in PBS, treated with Triton X-100 (Sigma) 1 % for 15 minutes at room temperature and incubated in mouse normal serum 1:20 for 40 minutes at room temperature. Then, slices were incubated at 4 °C overnight in humid chamber with primary monoclonal antibody. Next, tissues were washed in PBS, incubated with the secondary antibody for 2 hs. at room temperature in the dark and rinsed in PBS.

Digital images were captured, through an objective lens 20x and 0.7NA, with a monochromatic Apogee Charge-Coupled Device (CCD) camera, 14 bits of color resolution, 768x512 sensor size, and 9x9 μm^2 pixel size, mounted on an Olympus BX50 optical microscope equipped with a mercury UV-lamp.

The CCD camera was controlled by a personal computer with an Intel Pentium II 350 MHz processor, 256 MB of RAM and 6 GB of hard-disc space, with a software developed in our laboratory [12]. Images were automatically obtained using this software after the setup of some basic parameters, which included, image dimensions (512x512 $pixel^2$), number of images (80), exposure time of the CCD (1 second) and time delay between one image and the next (20 seconds).

Preprocessing and data extraction was carried out in the calculus free software Octave 3.6. It consisted on BIAS IMAGE subtraction TO all images of the sequence and the classification by intensity thresholding of those pixels with intensities corresponding to fluorescence signal in the first image. The pair of values of each pixel and the interval of exposition time to UV-light were then save on text files for statistical data analysis in the statistical free software R 2.14.

The parameters of the models given by equations (1) to (4) were obtained optimizing each model by least square method. This was carried out by using a nonlinear regression tool of R 2.14 [9], which implements, among other, the nl2sol algorithm for numerical optimization [13]. This implementation of the algorithm allows to setup lower and upper bounds for the parameter estimators, which is useful to constrain the solutions in the optimization process to values that have a physical meaning. Therefore, all those parameter estimators that multiply the exponential functions were selected to be positive because they represent concentrations, and those

parameter estimators that are exponent of the exponential functions were selected to be negative because they represent decay-rate constants.

Additionally, a set of initial guesses of the parameter estimators had to be passed to the algorithm. These initial guess were obtainded from data in order to automate the process. For models given by equations (1) and (2), the initial guess of the parameter θ_1 was setup to be the intensity value of the sequential data set at time zero. θ_2 was obtained as the first numerical difference between the two first intensity values. θ_3 is the background mean-level measured in a portion of the image without fluorescent signal. In models represented by equations (3) and (4), the initial values θ_1 and θ_3, were considered to be 50% of the first value of the sequence data set. θ_2 and θ_4 were obtained with numerical differences, between the first and second values and between the two last values of the sequence data set, respectively. Finally, θ_5 was measured from a region without fluorescent signal.

RESULTS AND DISCUSSION

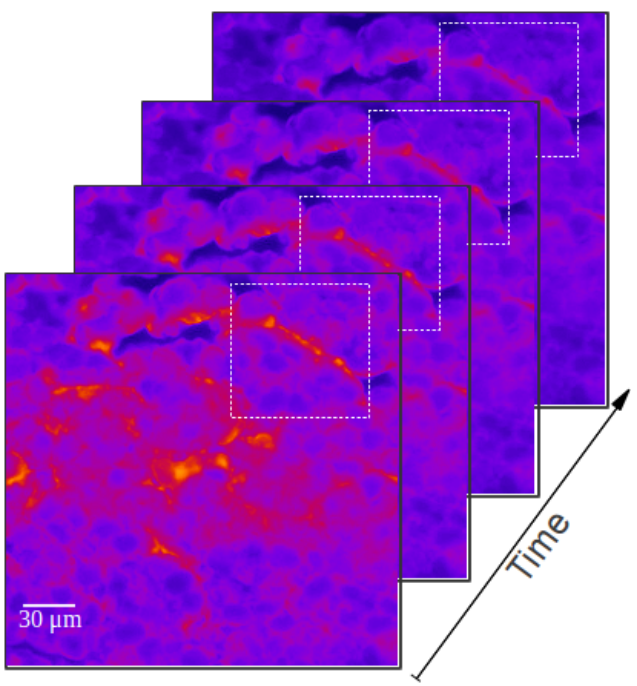

Fig. 1. Schematic representation of four pseudo colored images of the temporal sequence (256x256, 20x).

Fig. 1 is a schematic picture gallery of the temporal sequence obtained. The white dashed lines are spatially coincident and enclose the regions of interest (ROI) used to resume results in this report. Images were colored with a *fire* pseudo color lookup table in order to highlight differences on intensities that are not easily recognized by visual inspection on gray scale images.

Fig. 2 shows the ROIs indicated on Fig. 1 of five selected images of the full temporal sequence. The spatially coincident sub ROIs in white dashed line is a representation of the kernel size used for averaging neighbor pixels.

The set of averages obtained by processing each coincident sub ROI along the full temporal sequence were fitted to equations (1) to (4) as described en M&M section. Fig. 3 shows the fitted curves (red) to data (black) for each model. Equation (1) is a model that has been used in several works [14-18], and even when a graphical analysis evidences the poor fit (clearly, residuals has not normal distribution), the results obtained have been sufficient and satisfactory for the applications.

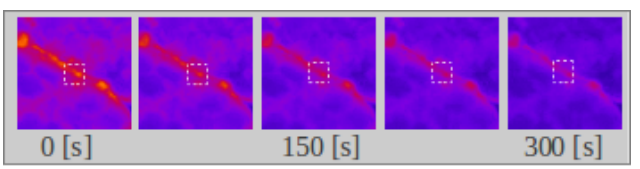

Fig. 2. Five pseudo colored images selected from the sequence of 80 (32x32, 20x).

Except for intensity decay given by equation (1), it is evident that is not possible to objectively establish which model is adequate only using the graphic representations, since superficially all of them fitted well. Analyzing the sum of square residuals (see table 1) can be seen that models given by equations 3 and 4 are which exhibit less residual sum. Even when these results give us some

information about which models can be the best to describe the data, they do not allow to objectively decide for any of them.

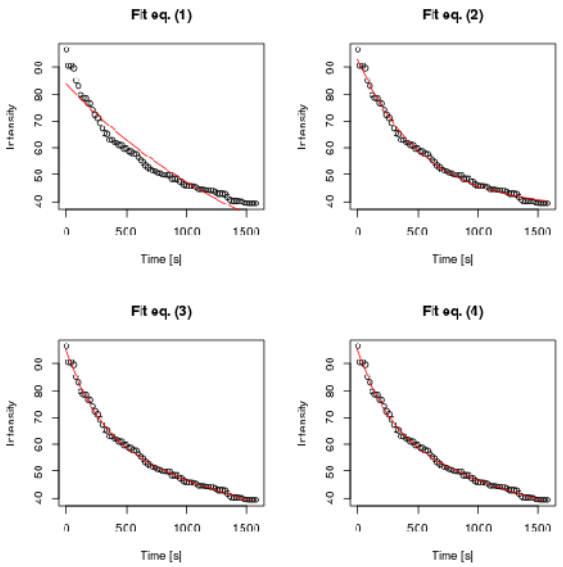

Fig. 3. Fitting graphs of models given by equations (1), (2), (3) and (4).

Table 1. Sum of standard residuals of the models

Model	*RSS(θ)/df*
Equation (1)	3.67
Equation (2)	1.08
Equation (3)	0.77
Equation (4)	0.77

For this reason, to objectively establish which model is the better one to represent the data, it was estimated the statistic F for each model combination, starting from more general models toward the simpler. Table 2 do resume the F-test results, corresponding to the comparison of the models given by equations (3) and (4) and following, by equations (3) and (2). We also carried out the comparisons of the all other model combinations, but as was expected, due to the nesting, model given by equation (3) significantly diminished the residual sum respect to the simpler models.

Table 2. *p*-values of the F-test applied to model comparisons

Model comparison	*p*-value
Eq. (3) vs. Eq (4)	0.6999
Eq. (2) vs. Eq (3)	3.268e-13

As can be observed at Table 2, model given by equation (4) did not introduce any significant change respect of equation (3), that mean that $\theta_5 = 0$, from which the complexity can be reduced to four parameters. The fitting of equation (3) showed significant differences compared to the fitting of equation (2) and so $\theta_4 \neq 0$. For this reason it can be deduced that this is the best model, of the set proposed, to describe the data.

Additionally, the estimator distributions were analyzed applying the bootstrap approach to the residuals obtained in each fitting [19]. Fig. 4 shows the distribution of the parameter estimator for model given by equation (3). In this figure the unimodal and approximately Gaussian shape of the parameter estimators can be observed and also their relationship in dispersion plots with the curves of the confidence intervals at 95%.

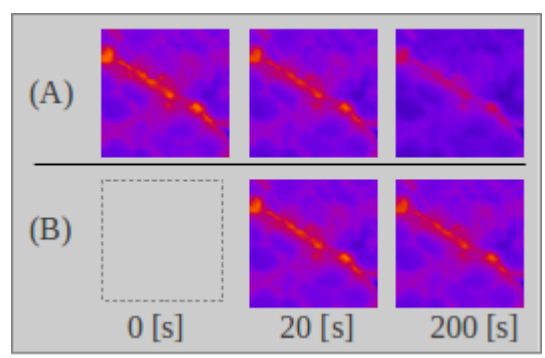

Fig. 4. Photobleaching correction applied to two images of the sequence. (A) Original images, (B) corrected images.

The parameter's estimator for the models given by equations (1), (2) and (4) were not adequately distributed.

Finally, a Shapiro-Wilk test of normality was applied to the residuals of all the models, being the model of equation (1) the only that showed significant differences from the normality condition.

Finally, Fig. 5 shows a correction applied using equation (3) to selected ROIs of the sequence. This recovery processing is illustrative and requires a deep evaluation and comparison with the other models.

CONCLUSIONS

The present report shows an objective way to choice, between several nonlinear models, the best that describe the data of the intensity decay due to photobleaching in fluorescence microscopy temporal series. This selection criterion is based on a F-test and requires that the non linear models are nested. In this work we have proposed four models finding that the bi-exponential without constant term, exhibit the best fitting to the data in the sense of the least square.

It is important to highlight that the mono-exponential model is still the most used [14-18], but this model do not fit adequately the data and this fact should be take into account when the recovery techniques will be used for signal or data normalization.

Future efforts will be directed to apply a photobleaching analysis to three dimensional fluorescence microscopy images obtained by optical sectioning [20], were the photobleaching is dependent of the specimen thickness and the spatial distribution of the excitation light.

As final conclusion, it should be clarified that the bi-exponential model without constant term, does not explain the photobleaching phenomena in a general form, due to this depend on several factors and requires a deep biophysical study of the tissue and its interaction with UV-light.

ACKNOWLEDGMENTS

Research reported in this publication was supported by federal funds obtained through the financing instrument PICT-O: 2009-0209 "*Rol de la adhesión celular en la morfogénesis y el mantenimiento de la arquitectura epithelial*". The content is solely the responsibility of the authors and does not necessarily represent the official views of the State's funding programs.

REFERENCES

[1] Lichtman J. W. and Conchello, J.-A (2005) "Fluorescence microscopy" *Nature Methods*, 2: 910-919.

[2] Wolf, D. E (2007). "Fundamentals of fluorescence and fluorescence microscopy" *Methods In Cell Biology*. 81: 63-91.

[3] Song L., Hennink, E. J., Young I. T. and Tanke H. J. (1995) "Photobleaching kinetics of fluorescein in quantitative fluorescence microscopy" *Biophys J.* 68: 2588-2600.

[4] Markham J. and Conchello J. A. (2001) "Artifacts in restored images due to intensity loss in three-dimensional fluorescence microscopy" *Journal of Microscopy, 204:* 93-98.

[5] Benson D. M., Bryan J., Plant A. L. Gotto A. M. and Smith L. C. (1985) "Digital imaging fluorescence microscopy: spatial heterogeneity of photobleaching rate constants in individual cells" *J Cell Biol, 100:*1309-1323.

[6] Vicente N. B., Diaz-Zamboni J. E., Adur J. F.; Paravani E. V. and Casco V. H. (2007). "Photobleaching correction in fluorescence microscopy images". *Journal of Physics: Conference Series, 90:* 012068.

[7] Bates D. M. and Watts D. G (1988). "Nonlinear Regression Analysis and Its Applications". *John Wiley & Sons.*

[8] Weisberg S. (2005). "Applied linear regression". *Wiley-Interscience,* 233-248.

[9] Ritz C. and Streibig J. C. (2008) "Nonlinear regression with R". *Springer.*

[10] Rengel D., Paz D., Pisano A. and Pasina L (1988) "Developmental capacity of Bufo arenarum aged ovocytes" *Microscopia Electrónica y Biología Celular,* 10:101-113.

[11] Gosner K. L (1960) "A Simplified table for staging anuran embryos and larvae with notes of identification" *Herpetologica, 16:*183-190.

[12] Diaz-Zamboni, J. E (2004). Software para usuarios de microscopios de desconvolución digital. Tesis de grado. Facultad de Ingeniería, Universidad Nacional de Entre Ríos.

[13] Dennis J. E., Gay D. M. and Walsh R. E. (1981) "An Adaptive Nonlinear Least-Squares Algorithm", *ACM Trans. Math. Softw*., 7:348-368.

[14] Ghauharali R. J., Hosftraat J. W. and Brakenhoff, G. J. (1998) "Fluorescence photobleaching-based shading correction for fluorescence microscopy", *Journal of Microscopy*, 192:99-113.

[15] Ghauharali R.J. and Brakenhoff G. J. (2000) "Fluorescence photobleaching-based image standardization for fluorescence microscopy", *Journal of Microscopy*, 198:88-100.

[16] Rodrigues I. and Sanches J. (2009). "Fluorescence microscopy imaging denoising with log-Euclidean priors and photobleaching compensation", *Image Processing (ICIP), 2009 16th IEEE International Conference on,* 809-812.

[17] Jezierska A., Talbot H., Chaux C., Pesquet J., and Engler G (2012). "Poisson-Gaussian noise parameter estimation in fluorescence microscopy imaging". Biomedical Imaging (ISBI), 9th IEEE International Symposium 1663 -1666.

[18] Hua Y. (2012). "Study of synaptic vesicle cycling during exo- and endocytosis using optical approaches". PhD Thesis, Georg-August-Universität Göttingen.

[19] Efron B. and Tibshirani R. J. (1993) "An Introduction to the Bootstrap" *Chapman & Hall/CRC,* 113-116.

[20] Conchello J.A. and Lichtman J. W (2005) "Optical sectioning microscopy" *Nature Methods,* 2:920-931.